Rhythmic Extended Kalman Filter for Gait Rehabilitation Motion Estimation and Segmentation

Vladimir Joukov, Vincent Bonnet, Michelle Karg, Gentiane Venture, and Dana Kulić, *Member, IEEE*

***Abstract*— This paper proposes a method to enable the use of non-intrusive, small, wearable, and wireless sensors to estimate the pose of the lower body during gait and other periodic motions and to extract objective performance measures useful for physiotherapy. The Rhythmic Extended Kalman Filter (Rhythmic-EKF) algorithm is developed to estimate the pose, learn an individualized model of periodic movement over time, and use the learned model to improve pose estimation. The proposed approach learns a canonical dynamical system model of the movement during online observation, which is used to accurately model the acceleration during pose estimation. The canonical dynamical system models the motion as a periodic signal. The estimated phase and frequency of the motion also allow the proposed approach to segment the motion into repetitions and extract useful features, such as gait symmetry, step length, and mean joint movement and variance. The algorithm is shown to outperform the extended Kalman filter in simulation, on healthy participant data, and stroke patient data. For the healthy participant marching dataset, the Rhythmic-EKF improves joint acceleration and velocity estimates over regular EKF by 40% and 37%, respectively, estimates joint angles with 2.4° root mean squared error, and segments the motion into repetitions with 96% accuracy.**

***Index Terms*— Human motion estimation, inertial measurement unit, motion model learning, gait rehabilitation.**

I. Introduction

PHYSIOTHERAPY is a type of rehabilitation that aims to restore a patient's quality of life after an injury, surgery, or stroke by improving their mobility. Through prescribed exercises and specialized equipment, physiotherapy helps the patient to regain their muscle strength, range of motion, and natural movement. Of particular interest in many rehabilitation regimens is gait, as improvements to locomotion are a key skill for improving functional ability and quality of life for patients. During gait rehabilitation, physiotherapists need a method for assessing patient performance. Currently physiotherapists rely on observational gait analysis that has been shown to have high inter-rater variability even among experts [1] and to have fairly low agreement with motion capture kinematics data [2]. Force plates can provide objective measures such as stride length, stance and swing duration [3], but do not provide an estimate of joint angles. A common technique for joint assessment is goniometry [4] that measures the total range of motion of a specific joint; however, it cannot be applied while the patient is performing an exercise and does not capture the overall motion of the patient. Lavernia *et al.* [5] evaluated the accuracy of therapist observation and goniometry measurements for knee range of motion assessment using x-ray imaging. Their analysis shows that on average physiotherapists tend to underestimate the range of motion by 9° relying purely on observation and by 7° when using a goniometer. Apart from being inaccurate, both goniometry and observational analysis are not very useful in tracking the patient's progress over time. Goniometry can only show increase in joint motion ranges and does not capture correctness of gait, balance improvement, or movement speed. Observational analysis is difficult to quantify and compare over multiple sessions.

Injuries or illnesses requiring physiotherapeutical treatment often afflict the elderly. In many developed countries the elderly population is rapidly growing. Demand for services related to care for the elderly, including physiotherapy, is expected to rapidly grow [6]. As the number of patients increases, therapists will not be able to work one on one with a patient and instead will supervise a group. Preventative and self-managed care is also expected to become more popular; patients will be expected to follow exercise regimens on their own time to manage chronic diseases, reduce hospital visits, and improve quality of life [6]. Patients are in need of tools to help them outside the clinic. Without feedback they may perform exercises incorrectly and prolong the rehabilitation period or even diminish their progress. An automatic assessment system that continuously tracks patient movement and is able to provide real-time feedback to both the therapist and the patient can improve patient motion performance and assist therapists with assessment, diagnosis, and treatment [7]. This system must achieve higher accuracy than goniometry, run in real-time for visual feedback, and segment exercises into repetitions to allow extraction of useful quantitative assessment measures.

Manuscript received April 7, 2016; revised November 8, 2016; accepted January 3, 2017. Date of publication January 26, 2017; date of current version February 9, 2018. *(Corresponding author: Vladimir Joukov.)*

V. Joukov, M. Karg, and D. Kulić are with the University of Waterloo, Waterloo, ON N2L 3G1, Canada (e-mail: jouk.vlad@gmail.com).

V. Bonnet is with the Université Paris-Est-Créteil, Laboratoire Images, Signaux et Systèmes Intelligents–EA 3956, Domaine Chérioux, 94400 Vitry sur Seine, France.

G. Venture is with the Graduate School of Engineering and Faculty of Engineering, Tokyo University of Agriculture and Technology, Tokyo 184-8588, Japan.

Digital Object Identifier 10.1109/TNSRE.2017.2659730

The proposed approach[1] allows for real-time joint angle estimation using small, wearable inertial measurement units worn at the ankles, knees, and waist to provide feedback to the patient and therapist as exercises are being performed. Furthermore, by combining the extended Kalman filter with a canonical dynamical system (CDS) the algorithm is able to learn periodic motion models over time improving estimation and to segment the exercises into repetitions. The segmentation allows extracting useful objective gait performance measures such as joint angle mean and variance, step length, and walking speed. Comparing the learned motion models over multiple therapy sessions can be used for patient progress tracking.

II. Related Work

Zhou *et al.* compared different technologies proposed for pose estimation in a rehabilitation setting. Inertial sensors were shown to be highly accurate, compact, and cost effective [9]. Most inertial sensors contain a MEMS accelerometer and gyroscope though some incorporate magnetometers and surface electromyography. To allow for real-time processing the sensors stream data through a wireless link to a workstation. Bergman analyzed preferences of clinicians and patients to determine design criteria for wearable non-invasive rehabilitation sensors [10]. Patients focus on the size and aesthetics of the sensor. They prefer small devices with sleek designs that do not affect normal daily behavior and are simple to use. Clinicians would like a system that provides them with information about patient progress, monitors the patient at home reducing hospital visits, and is simple to use. Wearable wireless inertial measurement units (IMUs) fit the desired design criteria perfectly. With advancements in microelectromechanical system (MEMS) manufacturing they can be made very small to not restrict the patient's movement, can wirelessly stream data in real time to provide feedback, and work in any environment [11]–[13].

It is possible to use inertial sensors to estimate position and orientation of each link independently, ignoring human kinematics, by integrating the gyroscope signal to obtain orientation of the link and double integrating the accelerometer signal to estimate position [14], [15]. Unfortunately, drift in the gyroscope signal and numerical integration inaccuracies lead to large error in the estimate over time.

Making assumptions about the performed motion can be useful to reduce the effect of drift. For gait, segmentation into stance and swing phases can be utilized. Various approaches for segmenting gait into cycles using foot worn inertial sensors have been proposed, including gyroscope signal thresholding [14], [15], hidden Markov models [16], and time warping techniques [17]. After segmentation, strap down integration can be used during the swing phase to estimate position and orientation and drift is compensated during the stance phase to improve tracking [14], [15]. Assuming the motion is periodic it is possible to use a weighted Fourier linear combiner to model gyroscope measurements and integrate the Fourier series into a drift free pose estimate [18]. This method however does not perform well without a priori knowledge of the motion until the weights are learned.

Without making any assumptions about the motion, a position based measurement can be used to reduce effects of gyroscope drift. Kortier relied on a permanent magnet worn on the hand and magnetometers on the trunk to aid with the orientation and position estimates [19]. Unlike GPS or visual based position tracking, their system can work indoors and does not suffer from occlusions, however, it may not be feasible with multiple patients in close proximity.

Using a human kinematic model allows estimation of not only link orientations but also joint angles and provides methods to enforce human movement constraints. Zhou *et al.* [20] employed strap down integration to compute the rotation of each link of the human arm and Lagrangian optimization to satisfy kinematic constraints. The optimization successfully deals with accelerometer drift due to double integration but does not reduce the gyro drift and requires computationally expensive regression. Schwarz *et al.* [21] approached the problem from a machine learning perspective. Using Gaussian Process Regression they learned a mapping between IMU sensor data and motion capture joint angles for each activity and individual separately. To determine what mapping to use when new sensor data is obtained they used a multi-class support vector machine to learn the classification of activities using sensor data. This method performs with an average joint angle error of 5.6°. Unfortunately this method only works well for the trained activities and does not generalize to the whole space of human motions. Also it cannot generalize to new subjects since the mappings for each activity must be learned per subject using a motion capture studio.

Lin and Kulić used a kinematic model and a Extended Kalman Filter (EKF) to estimate arbitrary 3D leg motion [22]. The states of the EKF are the joint positions, velocities, and accelerations, while the measurement vector consists of the accelerometer and gyroscope data from sensors attached above the knee and ankle. The EKF inherently deals with sensor noise and produces joint estimates directly, which can be used for real-time measurement and feedback [23]. To battle gyroscope drift potential fields were applied if the joint angle estimate left a defined range. Unscented Kalman filter was used by El-Gohary and McNames to estimate the shoulder and elbow joint angles however they did not implement kinematic constraints [24]. Both methods assume that the base of the kinematic model is fixed and cannot handle motions such as gait. The EKF approach can be extended to non-fixed base by switching the base of the kinematic model at each heel strike or representing the translation and rotation of the model with 3 prismatic and 3 revolute joints [25].

Apart from pose estimation, building an accurate model of the estimated motion is very useful for patient assessment and progress tracking. Comparing a learned model of the patient's movement with a healthy exemplar can be used as a measure of the patient's performance [26]. The motion model can also be used to improve pose estimation performance. It is possible to identify the performed motion by comparing it with

[1]In our previous work we introduced the algorithm [8] and performed validation in simulation and with healthy participants. In this paper, we extend the validation to include data collected in a longitudinal study with stroke patients and extract objective patient performance measures for therapists.

multiple known models. Segmentation into repetitions can be performed with a motion model that incorporates temporal features. To handle temporal and spatial variability in the motion, Ijspeert *et al.* used dynamic movement primitives (DMP) to model goal directed behavior with a non-linear system [27]. The dynamics of the motion trajectory are represented as a linear spring damper system with a learned non-linear forcing term. This approach is useful due to scaling and invariance properties of the model. Scaling the time constant and forcing terms does not effect the shape of the trajectory but changes the speed and spatial scale. The forcing term can also be used for motion identification by comparing the learned weights of known motions with a previously unseen motion. A rhythmic version of DMP was also developed based on a limit cycle system and online learning approaches have also been proposed [28].

A combination of an online rhythmic learning model based on Fourier series and DMP has been proposed by Gams *et al.* [29]. The performed rhythmic motion is modeled as a sum of multiple adaptive frequency phase oscillators and the lowest non-zero frequency oscillator is used as the phase in learning the rhythmic DMP. The DMP invariance properties are later used to reproduce scaled versions of the motion. Petrič*et al.* [30] noted that using multiple oscillators with different frequencies makes the adaptation process more difficult and learning the DMP is redundant in the system. Instead they used a harmonic Fourier series with a single base frequency and phase.

To the best of our knowledge, there is no approach that combines pose estimation with motion model learning. We model a patient's lower body using branched kinematics and combine an online periodic motion learning method [30] with the extended Kalman filter to develop a pose estimation algorithm which can learn the motion model online and use the model to improve pose estimation for periodic exercises such as gait. The algorithm also accurately segments rhythmic exercises into repetitions. In our preliminary work [8] we introduced the algorithm and the approach was validated in simulation as well as healthy participant data. In this paper, we evaluate the proposed approach through a longitudinal study collecting monthly gait assessment data from stroke patients undergoing rehabilitation treatment in a clinical setting. The proposed approach was used to estimate pose and segment the motion into repetitions. Objective measures for the physiotherapists including range of knee motion, symmetry between legs, stride length, and exercise execution time were extracted. These can greatly improve the therapists' ability to asses and monitor patients. The algorithm is shown to track joint angles to 2.4°.

III. Pose Estimation Method

In order to estimate joint angles useful for therapists and satisfy human movement constraints we model the human body using branched kinematics. To estimate the model's pose in real time using data from inertial measurement units worn at the ankles, knees, and waist, the extended Kalman filter is combined with a canonical dynamical system (CDS). The system incrementally learns the rhythmic motion over time, improving the estimate over a regular EKF by removing the constant acceleration assumption, and segmenting the motion into repetitions. A virtual yaw sensor is used to eliminate gyroscope drift. The phase and frequency variables estimated by the CDS also allow extraction of useful features from the estimated motion, which can be used to evaluate gait properties and isolate gait segments.

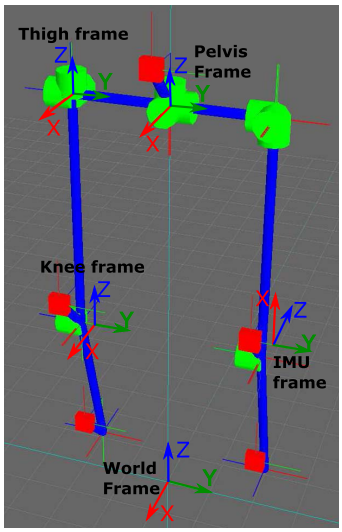

Fig. 1. Lower body model, red boxes represent attached IMUs and green cylinders are revolute joints of the model. The hip is modeled as three revolute joints to simulate a ball joint and the knee is a revolute joint, allowing for estimation of 3 dimensional human motion.

A. Lower Body Modeling

The human lower body is modeled as a set of rigid bodies connected through revolute joints to describe the motions achievable at the hips (ball joints) and knees (hinge joints). Each revolute joint defines a rotation about a single axis, constant transformation matrices define the rotation and translation between consecutive joints in the kinematic model. Five rigidly attached IMUs are located at the lower shank, lower thigh and lower trunk levels (Fig. 1). To model the translation and rotation of the pelvis, three prismatic and revolute joints connect it to the inertial frame [25].

With the frames assigned we can use forward kinematics to compute the position, velocity, and acceleration of each frame using those of the previous frame recursively. In the following, all the quantities are described in frame i of the kinematic model. To convert quantities from the previous frame $i-1$ to frame i the rotation matrix $R^i_{i-1}(q_i)$, composed of the constant transformation between consecutive joints and rotation due to the i_{th} joint, is used. Considering the angular velocity of the previous frame $\boldsymbol{\omega_{i-1}}$ and the joint velocity $\dot{q}_i$ caused by actuation of the joint i, the angular velocity of the current frame can be computed as

$$\boldsymbol{\omega}_i = \boldsymbol{\omega}_{i-1} + \xi_i \boldsymbol{b}_i \dot{q}_i \tag{1}$$

where $\boldsymbol{b}_i$ is the axis the joint acts upon and ξ_i defines the joint type (0 for prismatic, 1 for revolute). Taking the derivative of (1) the angular acceleration is:

$$\boldsymbol{\alpha}_i = \boldsymbol{\alpha}_{i-1} + \xi_i (\boldsymbol{b}_i \ddot{q}_i + \boldsymbol{\omega}_i \times \boldsymbol{b}_i \dot{q}_i) \tag{2}$$

The linear velocity at the end of link i can be calculated using the cross product of angular velocity and the displacement vector from this frame to the next $\boldsymbol{r}_i^{i+1}$ as

$$\dot{\boldsymbol{x}}_i = \dot{\boldsymbol{x}}_{i-1} + \boldsymbol{\omega}_i \times \boldsymbol{r}_i^{i+1} + (1-\xi_i)\boldsymbol{b}_i\dot{q}_i \tag{3}$$

Taking the derivative and adding gravity in the current frame, the linear acceleration at the end of link i is:

$$\begin{aligned}\ddot{\boldsymbol{x}}_i = \ddot{\boldsymbol{x}}_{i-1} + \boldsymbol{\alpha}_i \times \boldsymbol{r}_i^{i+1} + \boldsymbol{\omega}_i \times \boldsymbol{\omega}_i \times \boldsymbol{r}_i^{i+1} \\ + (1-\xi_i)(\boldsymbol{b}_i\ddot{q}_i + 2\boldsymbol{\omega}_i \times \boldsymbol{b}_i\dot{q}_i) + R_0^i(\boldsymbol{q})\boldsymbol{g}\end{aligned} \tag{4}$$

where $R_0^i(\boldsymbol{q})$ is the rotation from world frame to current frame computed using forward kinematics and $\boldsymbol{g}$ is the gravity vector. In the knee and thigh frames, the angular velocity vectors $\boldsymbol{\omega}$ and the linear acceleration vectors $\mathbf{R}$ are measured by the IMUs.

B. Rhythmic Extended Kalman Filter for Kinematic Chain

The Kalman Filter is a popular sensor fusion technique that estimates the state of a system from noisy observations. For a linear model, it is shown to be an optimal filter under the assumption that both measurement and process noise are zero-mean Gaussian [31].

For a non-linear system, state $\mathbf{s_t}$ and measurement $\mathbf{z_t}$, at time step t, are defined by

$$s_t = f(\mathbf{s}_{t-1}) + \mathbf{w}_{t-1} \tag{5}$$

$$\mathbf{z}_t = h(\mathbf{s}_t) + \mathbf{v}_t, \tag{6}$$

f is the nonlinear dynamic model relating the previous state to the next and h relates the measurement to the state. $\mathbf{w}$ and $\mathbf{v}$ are zero-mean Gaussian process and measurement noise with covariances Q and R respectively.

The Extended Kalman Filter linearizes the equations about the operating point. The equations are approximated as

$$\mathbf{z}_t \approx \tilde{\mathbf{z}}_t + \mathbf{C}(\mathbf{s}_t - \tilde{\mathbf{s}}_t) + \mathbf{v}_t \tag{7}$$

$$\mathbf{s}_t \approx \tilde{\mathbf{s}}_t + \mathbf{A}(\mathbf{s}_t - \tilde{\mathbf{s}}_t) + \mathbf{w}_{t-1}, \tag{8}$$

where $\mathbf{A}$ and $\mathbf{C}$ are the Jacobians of the state update and measurement equations with respect to the state $\mathbf{s}$, $\tilde{\mathbf{s}}$ is the noiseless state estimate, $\tilde{\mathbf{z}}$ is the noiseless measurement estimate, $\mathbf{v_t}$ is the measurement noise, and $\mathbf{w}_{t-1}$ is the process noise. The filter calculates the optimal Kalman gain K that minimizes the error co-variance matrix $P = cov(\mathbf{s}_t - \hat{\mathbf{s}}_t)$ and at each iteration updates the state as

$$\hat{\mathbf{s}}_t = f(\hat{\mathbf{s}}_{t-1}) + K(\mathbf{z}_t - h(f(\hat{\mathbf{s}}_{t-1}))) \tag{9}$$

where $\hat{\mathbf{s}}_t$ is the Kalman state estimate at time-step t [31].

For our purposes, the state vector consists of the position $\mathbf{q}$, velocity $\dot{\mathbf{q}}$, and acceleration $\ddot{\mathbf{q}}$ of the joint angles and the measurement vector includes the 3D acceleration and angular velocity IMU sensor readings. The state at the next time-step is predicted by integrating the velocity and acceleration terms [22], assuming any change in the acceleration is part of the noise:

$$\mathbf{q}_t = \mathbf{q}_{t-1} + \dot{\mathbf{q}}_{t-1}\Delta t + \ddot{\mathbf{q}}_{t-1}\Delta t^2/2 \tag{10}$$

$$\dot{\mathbf{q}}_t = \dot{\mathbf{q}}_{t-1} + \ddot{\mathbf{q}}_{t-1}\Delta t \tag{11}$$

$$\ddot{\mathbf{q}}_t = \ddot{\mathbf{q}}_{t-1}, \tag{12}$$

where Δt is the time difference between measurements.

The assumption that the joint acceleration is constant leads to lag in the acceleration estimate, which propagates to the velocity and position estimates. Instead of a constant acceleration, we can add higher order terms such as jerk into the model and assume constant jerk.

$$\ddot{\mathbf{q}}_t = \ddot{\mathbf{q}}_{t-1} + \dddot{\mathbf{q}}_{t-1}\Delta t \tag{13}$$

$$\dddot{\mathbf{q}}_t = \dddot{\mathbf{q}}_{t-1} \tag{14}$$

Unfortunately IMU sensors cannot measure jerk and thus no extra information is available to improve the acceleration estimate.

Consider the case when the motion is rhythmic, such as human gait. Then we can assume jerk is a function $F(\Omega)$ of the phase Ω and frequency λ of the motion:

$$\dddot{\mathbf{q}}_t = F(\Omega) \tag{15}$$

$$\dot{\Omega} = \lambda \tag{16}$$

However, even with periodic movement, the phase and frequency of the movement can be modified significantly due to human variability. We propose to learn $F(\Omega)$ during online estimation by learning an analytically differentiable joint velocity model to gradually improve the performance of the EKF over time. We use the CDS to learn the underlying harmonic Fourier series of the joint velocity and use the second analytical derivative as the jerk $F(\Omega)$.

1) Canonical Dynamical System: The CDS is an estimator based on the harmonic Fourier series

$$\hat{y} = \sum_{i=1}^{n} \alpha_i cos(i\Omega) + \sum_{i=1}^{n} \beta_i sin(i\Omega) \tag{17}$$

where $\hat{y}$ is the state estimate, α_i and β_i are the Fourier coefficients, and Ω is the current phase. A feedback adaptive frequency phase oscillator is used to adapt the coefficients and phase to learn a rhythmic motion online.

$$\dot{\Omega} = \lambda - \zeta e sin(\Omega) \tag{18}$$

$$\dot{\lambda} = -\zeta e sin(\Omega) \tag{19}$$

$$\dot{\alpha_i} = \eta cos(i\Omega)e \tag{20}$$

$$\dot{\beta_i} = \eta sin(i\Omega)e \tag{21}$$

Where λ is the angular frequency, e is the error between actual and estimated values $e = y - \hat{y}$, and ζ and η are the frequency and coefficient learning rates respectively. The harmonic Fourier series sine and cosine coefficients are adapted proportionally to the error and their contribution at phase Ω [30]. In the phase space representation of the oscillator, perturbations tangential to the limit cycle will accelerate or slow down the phase. If the perturbation is periodic in nature, this acceleration is proportional to the difference in frequency between the perturbation and the oscillator. Thus the tangential component of the perturbation ($esin(\Omega)$) is used to synchronize the oscillator frequency to that of the perturbation [32]. The CDS has been shown to converge in multiple simulations and physical experiments [30].

To learn the rhythmic jerk $F(\Omega)$ using this method, actual jerk values are required, which are not available from the EKF estimated state. Noting that the Fourier series are infinitely

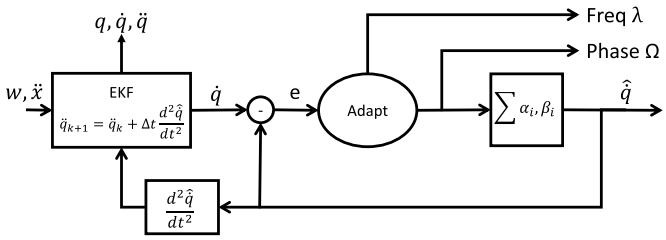

Fig. 2. Rhythmic-EKF Schematic

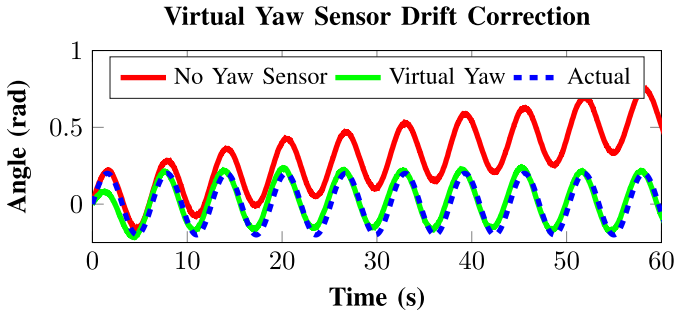

Fig. 3. Simulated EKF tracking of single joint angle which actuates about the world z axis and is measured by a biased gyroscope. The gyroscope has Gaussian noise with standard deviation of 0.05 rad/s and a constant bias of 0.01 rad/s. Without the virtual yaw sensor, EKF integrates the bias into the joint position estimate and error quickly accumulates. Once a virtual yaw sensor is added to the measurement vector it does not allow the joint position estimate to diverge without hindering accurate tracking of the out of plane rotation. The virtual yaw sensor measurement is set to a constant 0 and its noise standard deviation is tuned to 0.1 rad.

differentiable, the CDS can be used to learn the lower order terms, such as acceleration or velocity, and then analytically differentiate them to compute $F(\Omega)$. For pose estimation using IMU sensors, we choose joint velocity as the term to learn since it should be less affected by bias, and is not assumed to be constant, as is acceleration before the CDS is converged. The schematic of Rhythmic-EKF algorithm is presented in Fig. 2.

2) Virtual Yaw Sensor: The accelerometer's constant gravity reference ensures that EKF will accurately correct gyroscope drift coinciding with the real world x and y axis. However, EKF cannot correct gyroscope drift around the world z axis using the accelerometer data, this can result in accumulation of error in joint angle estimates for joints that rotate about axes parallel to the direction of gravity. To handle this issue, Lin and Kulić proposed applying potential fields in the EKF joint acceleration state once the joint position exceeds the joint limit [22]. The approach requires the potential field to be tuned for each joint independently and may cause oscillation of position estimate between the joint limits. Instead, we use a virtual yaw sensor γ as part of the measurement vector. It requires only a single tuning parameter and effectively combats gyro drift.

We assume that, for the most part, the human is walking in a straight line and thus the yaw angles of their pelvis and each thigh should not drift away from the original orientation. With this in mind, we attach a virtual yaw sensor to the pelvis and each thigh, the measurement is set to the starting orientation and is added as part of EKF measurement vector. The measurement noise of the virtual yaw sensor represents a soft constraint on the motion and is used as a tuning parameter. To allow for curved walking and turning, the pelvis yaw sensor can be removed and the thigh sensors can be set to measure yaw with respect to the pelvis frame instead of the world frame. In this case drift may accumulate in the estimate of the entire body orientation but the thigh rotation estimate will remain accurate.

Using forward kinematics the rotation matrix of the virtual sensor is computed. Expressing it in terms of the roll ρ, pitch τ, and yaw γ of the virtual sensor, the yaw angle measurement prediction can be computed from its entries as (22), as shown at the bottom of this page. The Jacobian of the yaw sensor is the third row of the velocity Jacobian [33] in the pelvis frame. Fig. 3 shows the benefits of using a virtual yaw sensor in EKF when the gyroscope measurement is biased. Note that the 3D motion is still observable and estimated, but the yaw sensor prevents the angle from drifting with time.

IV. Validation Methods

We use three different validation methods. First, to analyze the convergence and tracking improvement of Rhythmic-EKF over EKF, we analyze the pose estimation accuracy using simulated, perfectly periodic motions. Next, we show that Rhythmic EKF outperforms pose estimation for healthy participants and is able to accurately segment the rhythmic motion into repetitions. Finally, to verify that the algorithms can be used in a clinical setting, the performance on two stroke patients undergoing rehabilitation is demonstrated.

A. Simulation Validation

To test the convergence properties of Rhythmic-EKF, we simulate a gyroscope and an accelerometer attached at an offset of 0.5m to a single revolute joint rotating about the world x axis. To simulate periodic human motion, the joint is first actuated for 40 seconds using a Fourier series with 5 harmonics starting at 1 rads/s and coefficients from a univariate distribution. To test the algorithm's ability to adapt to changing frequencies, the frequency is continuously increased

$$R_{0,i} = \begin{bmatrix} cos(\gamma)cos(\tau) & cos(\gamma)sin(\tau)sin(\rho) - sin(\gamma)cos(\rho) & cos(\gamma)sin(\tau)cos(\rho) + sin(\gamma)sin(\rho) \\ sin(\gamma)cos(\tau) & sin(\gamma)sin(\tau)sin(\rho) + cos(\gamma)cos(\rho) & sin(\gamma)sin(\tau)cos(\rho) - cos(\gamma)sin(\rho) \\ -sin(\tau) & cos(\tau)sin(\rho) & cos(\tau)cos(\rho) \end{bmatrix}$$
$$\gamma = tan^{-1}\left(\frac{R_{0,i}(2,1)}{R_{0,i}(1,1)}\right) \quad (22)$$

from 1 to 5 rads/s. Using forward kinematics, the sensor measurements are computed and random Gaussian noise of $2\frac{m}{s}^2$ and $0.5\frac{rads}{s}$ is added to the accelerometer and gyroscope respectively. Next, the EKF's noise parameters that minimize the joint position estimation error are found using Matlab's constrained minimization toolbox. The Rhythmic-EKF uses the same noise parameters as the EKF; the number of harmonics as well as frequency and coefficient learning rates were chosen experimentally to be 7, 0.7, and 0.2 respectively. The initial frequency of Rhythmic-EKF is set to have an error of 15%. Starting the Fourier coefficients at zero guarantees initial performance of the Rhythmic-EKF is identical to that of the regular EKF and ensures no prior, possibly incorrect, assumption about the motion is made. We verify that the Rhythmic-EKF can successfully adapt the CDS to the rhythmic motion and we compare its performance to that of the EKF once convergence is achieved.

B. Healthy Participant Validation

Three subjects were asked to walk in place for two minutes while wearing 5 IMU sensors streaming at 50Hz and motion capture markers in a motion capture studio with eight cameras sampling at 100 frames per second. Three sets of data were collected: (1) Participants walking at 70 steps per minute using a metronome for timing, (2) walking at their own pace, and (3) walking using a metronome for timing and the metronome frequency was changed every 30 seconds. Three markers were placed on each of the sensors to determine their orientation and translation with respect to the link. Our IMUs are composed of MEMS accelerometer (ADXL345) and gyroscope (L3G4200D). Calibration was performed using the method described in [34] and the sensor axes were re-aligned with the three markers. Markers were also placed on the participants' left and right ASIS, backs, as well as knees and ankles on both medial and lateral sides. These markers were used to estimate the joint centers and link lengths to generate the kinematic model. The hip joint centers were determined using the pelvis width and length as well as leg length as described in Harrington *et al.* [35]. The position of the knee and ankle joint centres were obtained by taking the average of their respective medial and lateral marker positions. Data from the sensors and the motion capture was time-aligned in post processing. The study was approved by the University of Waterloo research ethics board.

Joint angles, velocities, and accelerations were obtained from marker data. The proposed Rhythmic-EKF algorithm was applied to the IMU data. For comparison, the pose was also computed using the control EKF algorithm, which does not utilize a model of the motion but instead applies the constant acceleration assumption [22]. Three virtual yaw sensors were added to the measurement vector at the center of the pelvis and each thigh to combat gyroscope drift. The noise parameters were tuned for the best performance of the EKF algorithm for the first participant. The Rhythmic-EKF was set to have 7 harmonics and the frequency and coefficient learning rates were set to 0.7 and 0.05 respectively. To verify the robustness of the motion model learning on real data, we performed a grid search that showed a wide range of frequency (0.5-4) and coefficient (0.05-1.5) learning rates will lead to convergence. To phase synchronize all of the joints, we use λ and $\mathbf{\Omega}$ estimated for the right knee joint for the entire lower body; the initial frequency was set to $5rad/s$ as an estimate of average walking speed. Since Rhythmic-EKF and EKF are expected to have the same performance during constant acceleration regions, we separately look at performance in the top 25% and bottom 75% joint acceleration regions.

C. Rehabilitation Patients Study

To evaluate the suitability of the proposed approach for pathological gait, data has been collected for two patients undergoing regular gait rehabilitation following a stroke in the hospital setting. Five monthly progress assessments were collected for patient 1, age 67, who suffered a hemorrhagic stroke and lost right side mobility. Four monthly progress assessments were collected for Patient 2, age 77, who suffered an ischemic stroke that affected his right side. Patient 2 had no previous morbidities but began experiencing hip pain in the paretic side towards the end of the rehabilitation period likely due to developing arthritis because of lost muscle strength. The study has been approved by University of Waterloo and Grand River Hospital research ethics boards. Specifically, IMU data was collected during a 6 minute walking task where the distance walked and step lengths are measured by the therapist. Data from each IMU was put through a low pass filter of 10Hz to eliminate accelerometer spikes during heel strikes. The kinematic model for each patient was defined using measured pelvis width, depth, and leg length. The same noise and CDS parameters were used as with healthy participants. Since no motion capture data is available to compute the transformation between each link and the IMU frames, a known initial static pose before gait was assumed and orientation with respect to each kinematic link was computed using the measured gravity vector. While the ankle IMU, placed on the shank, satisfies the rigid attachment assumption, the knee and waist sensors may experience slight movement on the body due to moving tissues. These motion artefacts are periodic in nature and are treated as additional measurement noise by the EKF.

Physiotherapists use the total distance walked during the 6 minute test, step length, and width as performance measures. While the distance walked d is trivial to measure, to get the patient's step length the physiotherapist tries to place coins at points where heel strikes occurred and measures the distance between them. Unfortunately this is a very error prone task as the exact spot where the patient stepped is not clear. Furthermore patients do not have perfect control of their muscles and thus step lengths are likely to have a high variance and the physiotherapists are only able to measure one or two steps due to time constraints. Using the phase variable provided by the Rhythmic-EKF, we segment the six minute walking task into discrete steps. It is then possible to calculate the average step length $\bar{l}$ as the largest distance between left and right ankle at each step. To verify that that the step length estimate is correct, we calculate the walking speed as $\lambda\bar{l}$ and compare it to the average walking speed as measured by the therapist.

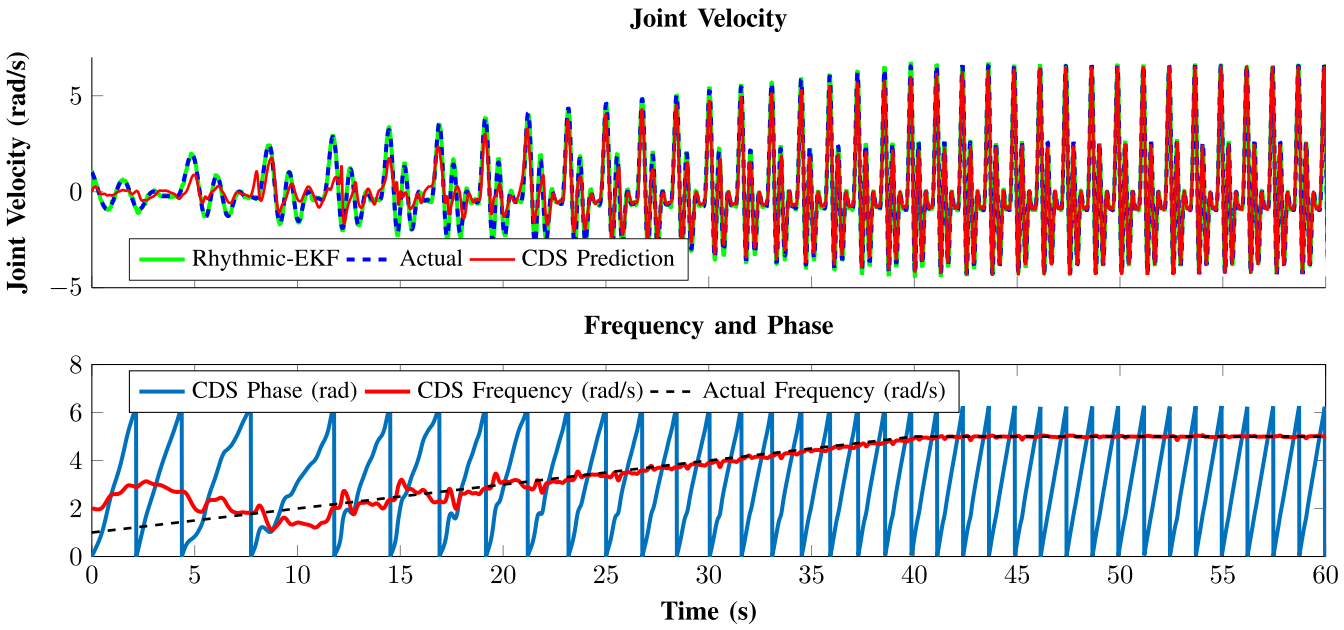

Fig. 4. Rhythmic-EKF convergence to rhythmic motion. The frequency, phase, and Fourier coefficients quickly adapt to accurately predict the joint velocity. Furthermore, it is able to track continuously changing frequency. The joint angle is estimated with a root mean squared error of 2.03° and 1.48° by EKF and Rhythmic-EKF respectively.

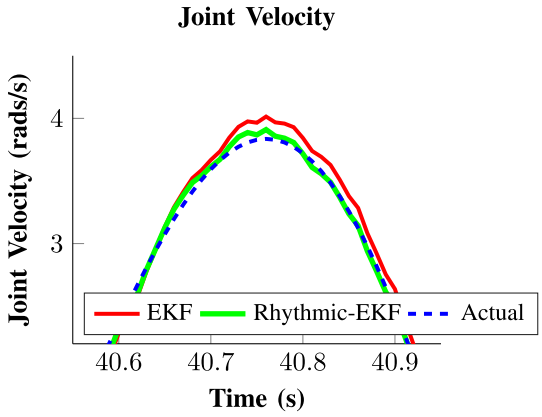

Fig. 5. Rhythmic-EKF performance during velocity peak compared to that of EKF after convergence is achieved. Since Rhythmic-EKF has an accurate model to predict acceleration the velocity estimate no longer overshoots or lags the actual value significantly.

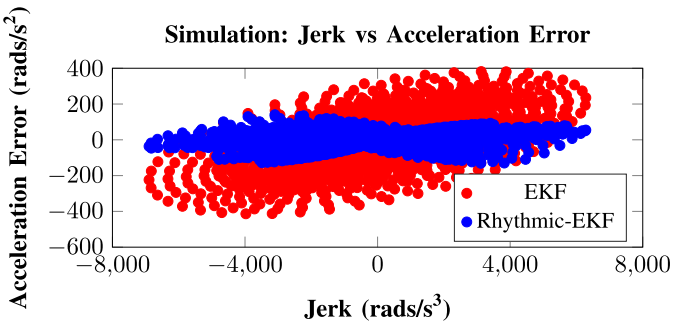

Fig. 6. Acceleration error plotted against jerk for the simulation presented in Fig. 4. Due to the constant acceleration assumption, EKF's estimated acceleration will always lag and the error will linearly increase with Jerk. This leads to an increase in the velocity, and position errors due to integration. After convergence Rhythmic-EKF has an accurate model of the acceleration profile and thus removes the lag and linear dependence on Jerk. This leads to an error distribution around zero.

V. Experimental Results

A. Simulation Results

In simulation the Rhythmic-EKF is able to quickly converge to the motion and significantly improve state estimation. Fig. 4 shows the adaptation process of the Rhythmic-EKF to the rhythmic motion. Frequency is accurately tracked after 10 seconds and the Fourier coefficients are learned within 10 repetitions of the motion. Furthermore, Rhythmic-EKF is able to track continuously changing frequency. A closer view of one of the velocity peaks after convergence is achieved is shown in Fig. 5. Since acceleration is no longer assumed constant, the predicted velocity does not overshoot or significantly lag the actual value.

The EKF's acceleration estimate error increases linearly with jerk since the model always predicts constant acceleration, the Rhythmic-EKF builds an accurate model over time, removing the constant acceleration assumption. Thus, by plotting jerk against error in acceleration estimate (Fig. 6), the benefits of the Rhythmic-EKF are very clear.

TABLE I
Mean Frequency After the Initial 15 Seconds of Walking Estimated by the Rhythmic-EKF

	Actual Freq (Hz)	Rhythmic-EKF Freq (Hz)	% Error
Subj1	1.167	1.170	-0.30
Subj2	1.167	1.179	-1.08
Subj3	1.167	1.169	-0.18

B. Healthy Participant Results

Fig. 7 shows Rhythmic-EKF convergence for a participant marching at their own pace. Table I shows the accuracy of the frequency convergence to the metronome trials after the first 15 seconds of walking. Even though human motion might

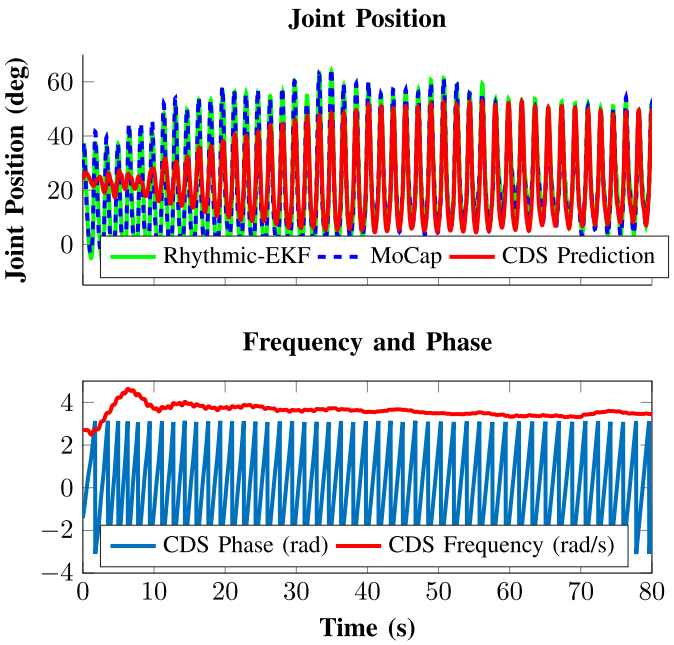

Fig. 7. Rhythmic-EKF convergence to self paced marching motion. Correct motion frequency is estimated after 5 repetitions. As soon as frequency is locked on, the Fourier coefficients begin to converge and start improving the estimate of jerk.

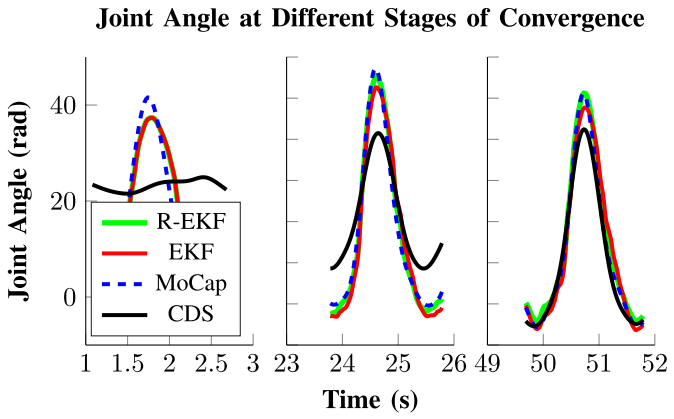

Fig. 8. At initialization (left) the Fourier coefficients of the CDS are set to zero, thus the estimated jerk is zero and Rhythmic-EKF and EKF perform identically. Even while the coefficients are in the process of being learned (middle) Rhythmic-EKF already has a better model than constant acceleration and performance is improved. Once the coefficients converge to a good model of the motion (right), Rhythmic-EKF significantly outperforms EKF in high acceleration regions.

not be perfectly periodic, the Rhythmic-EKF is able to find an underlying frequency and accurately track joint angles, velocities, and accelerations. At initialization, the Fourier coefficients of the CDS are zero resulting in zero estimated jerk and in the Rhythmic-EKF behaving identically to the regular EKF. The phase variable is initialized at zero and frequency is set to 5 rad/s, consistent with average human walking speed, for faster frequency convergence. Once the frequency is locked on, the Fourier coefficients are incrementally learned and the Rhythmic-EKF estimation outperforms that of the regular EKF. Fig. 8 shows the benefit of the Rhythmic-EKF at different stages of CDS Fourier coefficient convergence.

TABLE II

ROOT MEAN SQUARED ERROR AND STANDARD DEVIATION OF ERROR FOR THE JOINT POSITION, VELOCITY, AND ACCELERATION FOR HIP AND KNEE JOINTS (AVERAGED OVER LEFT AND RIGHT) OVER **TOP 25% ACCELERATION REGIONS**. STAR INDICATES RESULTS WHERE RHYTHMIC-EKF ERROR VALUES ARE SIGNIFICANTLY SMALLER THAN EKF

	Rhythmic-EKF		**EKF**	
	Joint Position RMSE (deg) ±STD(E) (deg)			
	Hip	Knee	Hip	Knee
Sub1	2.5±1.4	**2.4±1.6**	**1.9±1.3**	2.6±1.6
Sub2	**1.4±1.2***	**2.5±1.6***	2.1±1.3	3.0±2.0
Sub3	**3.7±1.5***	**2.0±1.9***	4.1±1.3	2.5±2.1
	Joint Velocity RMSE (deg/s) ±STD(E) (deg/s)			
	Hip	Knee	Hip	Knee
Sub1	**14.8±11.5***	**15.5±20.8***	18.9±12.5	29.3±27.5
Sub2	**6.6±9.5***	**23.9±21.7***	12.0±10.1	35.0±30.6
Sub3	**12.8±8.4***	**14.9±18.8***	18.7±9.1	29.4±26.7
	Joint Acceleration RMSE (deg/s^2) ±STD(E) (deg/s^2)			
	Hip	Knee	Hip	Knee
Sub1	**120.4±116.2***	**312.5±236.3***	277.1±114.3	587.2±272.8
Sub2	**80.4±86.2***	**339.4±227.4***	193.8±90.4	577.4±266.2
Sub3	**87.0±77.9***	**233.8±196.5***	190.5±83.9	421.8±242.4

TABLE III

ROOT MEAN SQUARED ERROR AND STANDARD DEVIATION OF ERROR FOR JOINT POSITION, VELOCITY, AND ACCELERATION FOR HIP AND KNEE JOINTS (AVERAGED OVER LEFT AND RIGHT) OVER **BOTTOM 75% ACCELERATION REGIONS**. STAR INDICATES RESULTS WHERE RHYTHMIC-EKF ERROR VALUES ARE SIGNIFICANTLY SMALLER THAN EKF

	Rhythmic-EKF		**EKF**	
	Joint Position RMSE (deg) ±STD(E) (deg			
	Hip	Knee	Hip	Knee
Sub1	1.9±1.4	2.0±1.6	**1.6±1.5**	**1.8±1.6**
Sub2	**1.4±1.1***	**2.8±1.5**	1.7±1.3	2.8±1.9
Sub3	**3.6±1.1***	**1.9±1.6**	4.1±1.2	1.9±2.1
	Joint Velocity RMSE (deg/s) ±STD(E) (deg/s)			
	Hip	Knee	Hip	Knee
Sub1	**11.9±8.7***	**13.37±17.7***	13.9±10.6	27.9±24.3
Sub2	**6.3±6.3***	**16.8±17.3***	9.4±8.7	30.3±23.3
Sub3	**11.2±5.5***	**12.8±15.0***	15.2±8.6	25.4±23.4
	Joint Acceleration RMSE (deg/s^2) ±STD(E) (deg/s^2)			
	Hip	Knee	Hip	Knee
Sub1	**103.9±80.9***	**155.4±139.4***	122.08±79.3	270.0±178.4
Sub2	**56.7±48.7***	**162.5±127.9***	80.6±53.3	247.8±153.8
Sub3	**71.4±50.8***	**122.8±118.0***	89.1±52.0	185.9±143.3

The above results were obtained during metronome trials, when participants were aurally cued to keep marching at a constant frequency. However, without metronome cueing, the gait frequency may not be constant. To investigate the behaviour of the system during normal gait, we next evaluate the proposed approach on our data set of participants walking at their own pace. Table II presents the hip and knee joint position, velocity, and acceleration root mean squared error (RMSE) over regions where absolute acceleration exceeds 75% of maximum. Even without noise parameters tuned for the Rhythmic-EKF, on average, the Rhythmic-EKF improves the velocity and acceleration estimation by 35% and 55% respectively in high acceleration regions. In low acceleration regions, the Rhythmic-EKF still outperforms EKF but the difference is not as drastic in acceleration estimation; Table III presents the RMSE for acceleration regions under

TABLE IV
RHYTHMIC-EKF'S AND EKF'S MEASUREMENT PREDICTION FOR THE NEXT TIME STEP COMPARED TO IMU DATA AVERAGED FOR LEFT AND RIGHT SIDES

	Rhythmic-EKF		**EKF**	
	Gyroscope RMSE (deg/s)			
	Knee IMU	Ankle IMU	Knee IMU	Ankle IMU
Sub01	**10.08**	**11.55**	17.52	21.23
Sub02	**10.69**	**13.05**	15.51	20.45
Sub03	**10.98**	**10.82**	18.78	23.08
	Accelerometer RMSE (m/s^2)			
	Knee IMU	Ankle IMU	Knee IMU	Ankle IMU
Sub01	**1.18**	**0.96**	1.35	1.18
Sub02	**1.18**	**1.05**	1.30	1.24
Sub03	**1.21**	**1.15**	1.34	1.48

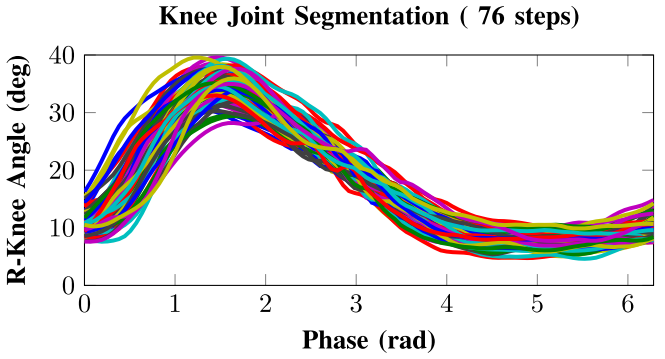

Fig. 9. Segmentation of estimated joint position using the phase of Rhythmic-EKF. The segmentation begins after 15 seconds of walking to allow Rhythmic-EKF to achieve convergence. Each color represents a segmented step cycle.

75% of maximum. In all the tables below, the results in bold indicate the best performing system for the corresponding row. The difference between the R-EKF and EKF is statistically significant, we conducted the one sided Kolmogorov-Smirnov test [36] concluding that for most of the results the results in tables II and III Rhythmic-EKF has a larger error cumulative distribution function and thus smaller error values.

The Rhythmic-EKF model also significantly improves measurement prediction which can be useful in control applications. Table IV shows the RMSE between actual and predicted gyroscope and accelerometer measurements for the next time step, after the first 15 seconds of walking for the knee and ankle IMU.

Once Rhythmic-EKF achieves frequency convergence the estimated phase can be used for segmenting the motion as well as temporally aligning the segments. We allow the algorithm to run for 15 seconds before using the phase variable for segmentation. Between the 3 participants a total of 306 steps were taken, there were 11 visibly incorrect segments in the hip joints and 7 in the knee joints leading to an accuracy of 96.4% and 97.1% respectively. Fig. 9 shows the right knee joint angle estimate segmented using the phase variable.

Due to quick convergence of the frequency and phase variables Rhythmic-EKF can handle changing frequencies. Fig. 10 shows tracking of the frequency and phase and motion segmentation based on the estimated phase for the

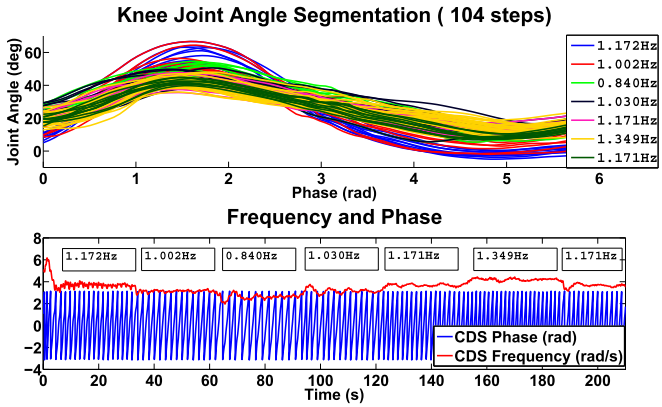

Fig. 10. Metronome walking trial where the frequency was changed every 30 seconds (1.167Hz, 1Hz, 0.833Hz, 1Hz, 1.167Hz, 1.33Hz, 1.167Hz). Rhythmic-EKF successfully tracks the variable frequencies. The top plot depicts segments temporally aligned and stretched using the phase variable. The bottom plot shows the frequency and phase tracking, as well as mean frequency estimated for each 30 second interval.

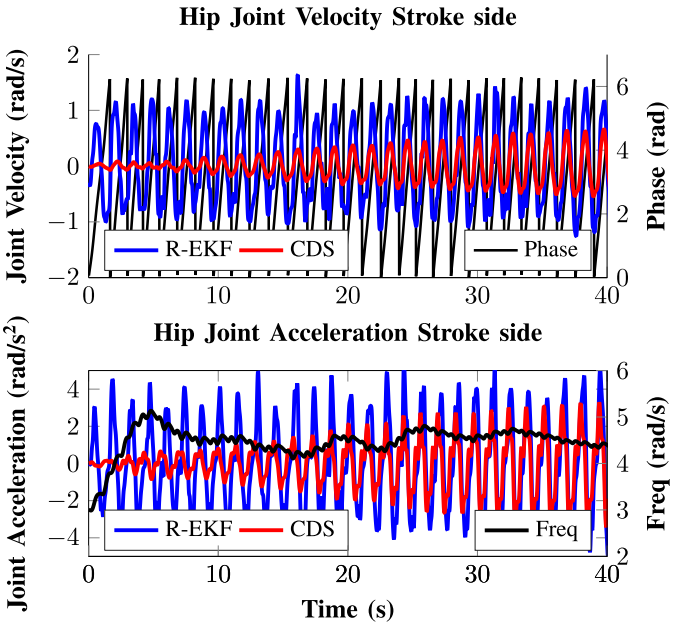

Fig. 11. Frequency converges to the patient's motion within 5 steps. The Fourier coefficients take longer to converge but begin to improve estimation as soon as frequency is converged.

varying metronome frequency trial. The algorithm was able to accurately track the frequency and phase of the motion. The phase was used for segmentation and temporal alignment.

C. Rehabilitation Patient Results

Despite significantly more variance in the motion due to missteps and weak muscle control, the Rhythmic-EKF successfully converges to the patients' motion and can be used for pose estimation and segmentation. Fig. 11 shows the convergence of Rhythmic-EKF to the patient's motion within only a few steps.

While we do not have access to motion capture data for comparison in the clinical setting, we can indirectly validate the pose estimation accuracy by using the estimated joint

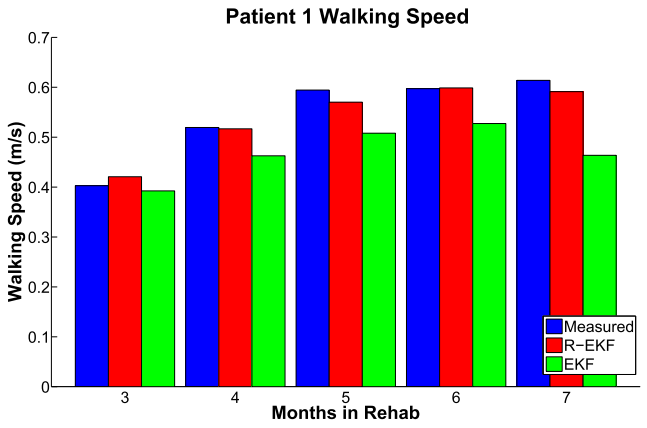

Fig. 12. Comparison of patient 1 measured and calculated walking speed. The walking speed is computed based on average frequency and step length as estimated by Rhythmic-EKF.

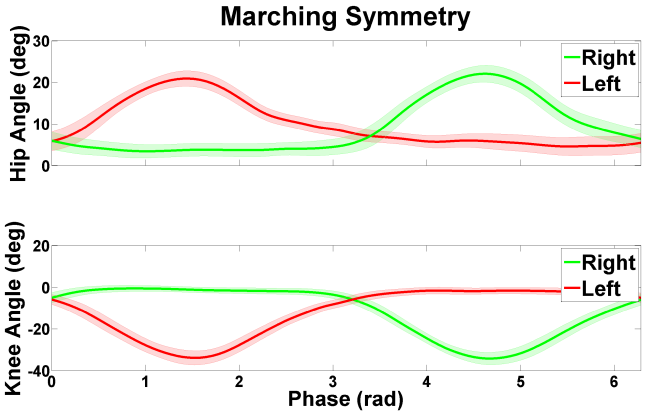

Fig. 14. Mean and standard deviation of the joint angle segments during marching at participant's own pace exercise. Accurate tracking of phase makes temporal alignment of the segments possible.

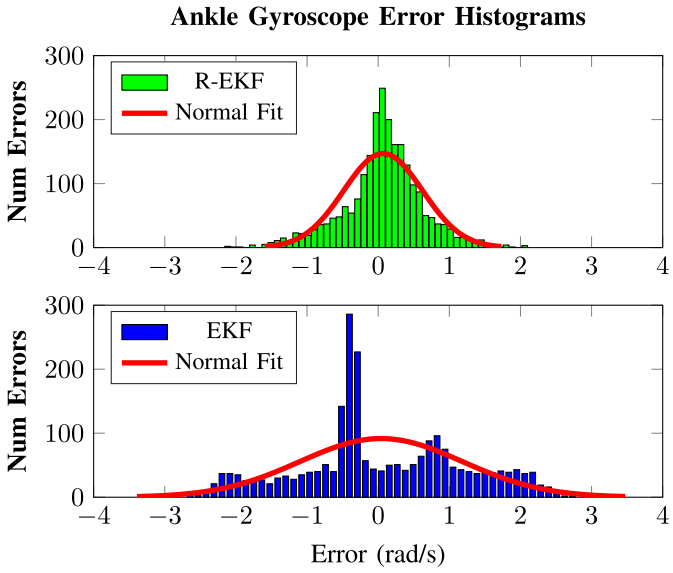

Fig. 13. Patient 1 Rhythmic-EKF and EKF ankle gyroscope error histograms. Rhythmic-EKF errors follow the zero-mean normal distribution closely showing that it has an accurate motion model.

angles and velocities together with the kinematic model to compute the walking speed. To accurately compute patient's walking speed we need precise estimates of the pose, frequency, and phase during the entire 6 minute test. Thus walking speed provides an indirect measure for the accuracy of the entire estimation and can be easily measured by therapists. Fig. 12 shows that the average step length and frequency calculated using Rhythmic-EKF provide an excellent estimate of the patients' walking speeds.

Another indirect measure of accuracy is the difference between predicted and actual measurements. With a correctly estimated motion model one expects the error between predicted and actual measurement to follow a zero-mean normal distribution due to random sensor noise. Fig. 13 shows the error histogram of the ankle gyroscope on the affected side for both Rhythmic-EKF and EKF over one of the walking tests.

VI. Discussion and Conclusion

In this paper we presented a novel method to estimate lower body pose during gait using data from wearable inertial measurement units. Previous methods consider the pose estimation and motion model learning as two separate steps. The developed Rhythmic extended Kalman filter algorithm is able to estimate pose and to learn a rhythmic motion model online and then use the learned model to improve pose estimation. It also estimates the phase and frequency of the movement.

The approach was validated in simulation, with healthy participant data, and with collected stroke patient gait assessment data. The simulation results showed that once Rhythmic-EKF converges to the motion, the tracking is improved for all states, i.e., the acceleration, position, and velocity over EKF with optimal noise parameters. Particularly lag, overshoot and undershoot in acceleration and velocity estimates are reduced. Rhythmic extended Kalman filter is able to estimate joint angles of healthy participant marching with 2.4° root mean squared error, significantly outperforming goniometry (RMSE 7° [37]) and visual observation (RMSE 9° [5]) techniques currently used by physiotherapists. Using the predicted phase variable the algorithm successfully segmented gait into repetitions with 96% accuracy.

With the motion segmented and the segments aligned based on the estimated phase, important measures such as mean and standard deviation of the joint trajectories can be extracted. Because all of the lower body joints are synchronized to the phase of a single joint, it is easy to visualize the symmetry between the left and right sides, which is very useful in physiotherapy. Fig. 14 shows the mean and standard deviation of hip and knee joint angles during the healthy participant marching exercise.

This makes Rhythmic-EKF a particularly well suited approach for gait rehabilitation. Using the estimated pose and frequency, walking speed can be computed accurately and used as a performance measure. Stroke patients often rely on a compensatory gait strategy due to lost muscle control and spasticity (muscle tone). Thibaut *et al.* [38] analyzed spasticity

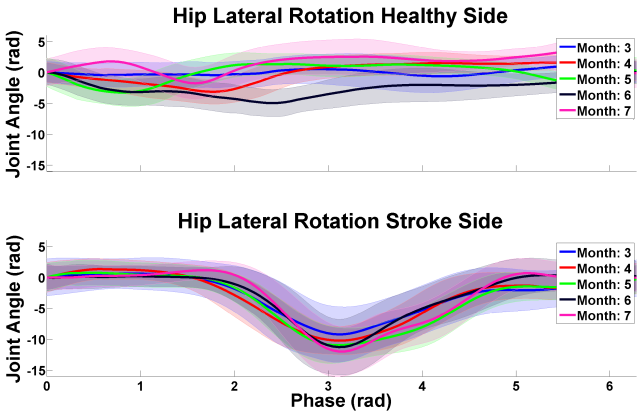

Fig. 15. Patient 1 hip lateral rotation strategy.

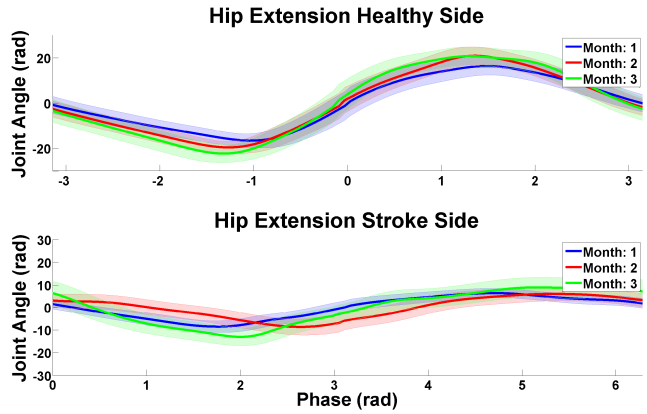

Fig. 16. Patient 2 healthy and stroke side hip extension comparison.

patterns in patients and their side effects. Spasticity patterns affecting gait are adducted thigh, stiff knee, flexed knee, and equinovarus foot. These may result in difficulties in limb clearing, extended knee and toe dragging during gait, short step lengths, and deviant knee flexion during pre swing. While simple measures such as an increase in speed and step length over multiple sessions shows a patient's improved ability to walk, they do not reveal whether the patient is regaining lost muscle control or is adopting a compensatory gait strategy. Understanding the compensatory strategies of a patient can help physiotherapists create specialized exercise regimens to regain muscle control and natural gait. We compute the average joint angles over a gait cycle for each monthly test. This leads to symmetry plots between the healthy side and paretic side. Fig. 15 shows the average hip lateral rotation over the rehabilitation period. It is clear that Patient 1 experiences the stiff knee spasticity pattern and that he did not recover natural gait over the rehabilitation period, instead he adopted a strategy to compensate for difficulty in knee flexion using hip lateral rotation.

Since gait patterns are individual specific it is hard to determine what defines a healthy cycle. For stroke patients therapists often compare the affected side to the healthy side as a measure of progress. Accurate estimate of phase allows shifting the gait cycle of one side by π for direct comparison. Fig. 16 shows the mean hip extension comparison between

TABLE V
JOINT ANGLE RMSE BETWEEN HEALTHY AND PARETIC SIDES OVER THE REHABILITATION PERIOD. DATA FOR PATIENT 2 MONTH 3 IS NOT AVAILABLE DUE TO A SENSOR FAILURE DURING THAT DAY'S MEASUREMENT SESSION

	Patient 1		Patient 2	
	RMSE between effected and healthy sides (deg)			
Month	Hip	Knee	Hip	Knee
1	4.03	13.51	12.98	12.19
2	10.23	18.56	11.58	13.64
3	10.87	19.23		
4	8.17	19.35	11.013	11.45
5	12.13	15.08		

the two sides. Calculating the joint angle root mean squared error between the two sides can help the therapist in patient assessment and progress tracking. Table V provides the hip and knee extension RMSE between healthy and stroke sides over the rehabilitation period. After the first assessment session patient 1 suffered from increased muscle tone and his performance did not improve. Patient 2 shows slight improvement in hip flexion and extension as seen in Fig. 16 and in the table, but no change in knee flexion.

In the future we will use the Fourier coefficients of the CDS to compare a patient's gait with healthy exemplars. This can provide an accurate progress measure over long recovery periods. Currently, for best performance the algorithm requires tuned process noise parameters, these are individual specific and thus the system may experience different performance between patients. An adaptive estimation of process noise in Rhythmic-EKF can be implemented. As the algorithm learns the rhythmic motion, it is expected that the state update prediction error decreases and thus the process noise parameters should adapt accordingly. An online adaptation of noise parameters is expected to significantly improve pose estimation. The prediction error can also be used to detect if the motion is becoming non-periodic and switching from Rhythmic-EKF to EKF. We will also explore using the estimated phase of the gait cycle to detect various gait cycle events of interest useful for patient evaluation and progress tracking, such as heel strike, swing, and toe off. Finally, applicability of Rhythmic-EKF to different periodic, almost periodic, and non periodic signals will be investigated.

REFERENCES

[1] J. J. Brunnekreef, C. J. T. van Uden, S. van Moorsel, and J. G. M. Kooloos, "Reliability of videotaped observational gait analysis in patients with orthopedic impairments," *BMC Musculoskeletal Disorders*, vol. 6, no. 1, p. 17, 2005.

[2] B. Toro, C. Nester, and P. Farren, "A review of observational gait assessment in clinical practice," *Physiotherapy Theory Pract.*, vol. 19, no. 3, pp. 137–149, 2003.

[3] T. Caderby, E. Yiou, N. Peyrot, B. Bonazzi, and G. Dalleau, "Detection of swing heel-off event in gait initiation using force-plate data," *Gait Posture*, vol. 37, no. 3, pp. 463–466, 2013.

[4] C. C. Norkin and D. J. White, *Measurement of Joint Motion: A Guide to Goniometry*. Philadelphia, PA, USA: F. A. Davis, 2009.

[5] C. Lavernia, M. D'Apuzzo, M. D. Rossi, and D. Lee, "Accuracy of knee range of motion assessment after total knee arthroplasty," *J. Arthroplasty*, vol. 23, no. 6, pp. 85–91, 2008.

[6] J. Jones, K. Norman, and S. Saunders, *The State of the Union: Trends and Drivers of Change in Physiotherapy in Ontario in 2014*. Kingston, ON, Canada: Queen's Univ., 2014. [Online]. Available: https://qspace.library.queensu.ca/handle/1974/12616?show=full

[7] A. W. K. Lam, D. Varona-Marin, Y. Li, M. Fergenbaum, and D. Kulić, "Automated rehabilitation system: Movement measurement and feedback for patients and physiotherapists in the rehabilitation clinic," *Human-Comput. Interaction*, vol. 16, nos. 3–4, pp. 294–334, 2016.

[8] V. Joukov, V. Bonnet, M. Karg, G. Venture, and D. Kulić, "Rhythmic EKF for pose estimation during gait," in *Proc. IEEE-RAS 15th Int. Conf. Humanoid Robots*, Nov. 2015, pp. 1167–1172.

[9] H. Zhou and H. Hu, "Human motion tracking for rehabilitation—A survey," *Biomed. Signal Process. Control*, vol. 3, no. 1, pp. 1–18, 2008.

[10] J. H. Bergmann and A. H. McGregor, "Body-worn sensor design: What do patients and clinicians want?" *Ann. Biomed. Eng.*, vol. 39, no. 9, pp. 2299–2312, 2011.

[11] C. A. Cifuentes *et al.*, "Evaluation of IMU ZigBee sensors for upper limb rehabilitation," in *Converging Clinical and Engineering Research on Neurorehabilitation*. Berlin, Germany: Springer, 2013, pp. 461–465.

[12] K. S. Low, G. X. Lee, and T. Taher, "A wearable wireless sensor network for human limbs monitoring," in *Proc. IEEE Instrum. Meas. Technol. Conf. (I2MTC)*, May 2009, pp. 1332–1336.

[13] A. Burns *et al.*, "SHIMMER—A wireless sensor platform for non-invasive biomedical research," *IEEE Sensors J.*, vol. 10, no. 9, pp. 1527–1534, Sep. 2010.

[14] A. M. Sabatini, C. Martelloni, S. Scapellato, and F. Cavallo, "Assessment of walking features from foot inertial sensing," *IEEE Trans. Biomed. Eng.*, vol. 52, no. 3, pp. 486–494, Mar. 2005.

[15] A. Rampp, J. Barth, S. Schülein, K. G. Gaßmann, J. Klucken, and B. M. Eskofier, "Inertial sensor-based stride parameter calculation from gait sequences in geriatric patients," *IEEE Trans. Biomed. Eng.*, vol. 62, no. 4, pp. 1089–1097, Apr. 2015.

[16] A. Mannini and A. M. Sabatini, "Gait phase detection and discrimination between walking–jogging activities using hidden Markov models applied to foot motion data from a gyroscope," *Gait Posture*, vol. 36, no. 4, pp. 657–661, 2012.

[17] J. Barth *et al.*, "Stride segmentation during free walk movements using multi-dimensional subsequence dynamic time warping on inertial sensor data," *Sensors*, vol. 15, no. 3, pp. 6419–6440, 2015.

[18] V. Bonnet, C. Mazzà, J. McCamley, and A. Cappozzo, "Use of weighted Fourier linear combiner filters to estimate lower trunk 3D orientation from gyroscope sensors data," *J. Neuroeng. Rehabil.*, vol. 10, no. 1, p. 29, 2013.

[19] H. G. Kortier, J. Antonsson, H. M. Schepers, F. Gustafsson, and P. H. Veltink, "Hand pose estimation by fusion of inertial and magnetic sensing aided by a permanent magnet," *IEEE Trans. Neural Syst. Rehabil. Eng.*, vol. 23, no. 5, pp. 796–806, Sep. 2015.

[20] H. Zhou, T. Stone, H. Hu, and N. Harris, "Use of multiple wearable inertial sensors in upper limb motion tracking," *Med. Eng. Phys.*, vol. 30, no. 1, pp. 123–133, 2008.

[21] L. A. Schwarz, D. Mateus, and N. Navab, "Discriminative human full-body pose estimation from wearable inertial sensor data," in *Proc. 2nd 3D Physiol. Hum. Workshop (3DPH)*, Zermatt, Switzerland, Dec. 2009, pp. 159–172.

[22] J. F. S. Lin and D. Kulić, "Human pose recovery using wireless inertial measurement units," *Physiol. Meas.*, vol. 33, no. 12, p. 2099, 2012.

[23] A. W. K. Lam, A. HajYasien, and D. Kulić, "Improving rehabilitation exercise performance through visual guidance," in *Proc. 36th Annu. Int. Conf. IEEE Eng. Med. Biol. Soc. (EMBC)*, Aug. 2014, pp. 1735–1738.

[24] M. El-Gohary and J. McNames, "Shoulder and elbow joint angle tracking with inertial sensors," *IEEE Trans. Biomed. Eng.*, vol. 59, no. 9, pp. 2635–2641, Sep. 2012.

[25] V. Joukov, M. Karg, and D. Kulić, "Online tracking of the lower body joint angles using IMUs for gait rehabilitation," in *Proc. 36th Annu. Int. Conf. IEEE Eng. Med. Biol. Soc. (EMBC)*, Aug. 2014, pp. 2310–2313.

[26] R. Houmanfar, M. Karg, and D. Kulić, "Movement analysis of rehabilitation exercises: Distance metrics for measuring patient progress," *IEEE Syst. J.*, vol. 10, no. 3, pp. 1014–1025, Sep. 2016.

[27] A. J. Ijspeert, J. Nakanishi, H. Hoffmann, P. Pastor, and S. Schaal, "Dynamical movement primitives: Learning attractor models for motor behaviors," *Neural Comput.*, vol. 25, no. 2, pp. 328–373, 2013.

[28] S. Schaal, J. Peters, J. Nakanishi, and A. Ijspeert, "Learning movement primitives," in *Robotics Research. The Eleventh International Symposium*, P. Dario and R. Chatila, Eds. Berlin, Germany: Springer, 2005, pp. 561–572.

[29] A. Gams, A. J. Ijspeert, S. Schaal, and J. Lenarčič, "On-line learning and modulation of periodic movements with nonlinear dynamical systems," *Auto. Robots*, vol. 27, no. 1, pp. 3–23, 2009.

[30] T. Petrič, A. Gams, A. J. Ijspeert, and L. Žlajpah, "On-line frequency adaptation and movement imitation for rhythmic robotic tasks," *Int. J. Robot. Res.*, vol. 30, no. 14, pp. 1775–1788, 2011.

[31] R. E. Kalman, "A new approach to linear filtering and prediction problems," *Trans. ASME D, J. Basic Eng.*, vol. 82, no. 1, pp. 35–45, 1960.

[32] L. Righetti, J. Buchli, and A. J. Ijspeert, "Dynamic Hebbian learning in adaptive frequency oscillators," *Phys. D, Nonlinear Phenomena*, vol. 216, no. 2, pp. 269–281, 2006.

[33] H. Bruyninckx and J. De Schutter, "Symbolic differentiation of the velocity mapping for a serial kinematic chain," *Mech. Mach. Theory*, vol. 31, no. 2, pp. 135–148, 1996.

[34] D. Tedaldi, A. Pretto, and E. Menegatti, "A robust and easy to implement method for IMU calibration without external equipments," in *Proc. IEEE Int. Conf. Robot. Autom. (ICRA)*, May/Jun. 2014, pp. 3042–3049.

[35] M. E. Harrington, A. B. Zavatsky, S. E. M. Lawson, Z. Yuan, and T. N. Theologis, "Prediction of the hip joint centre in adults, children, and patients with cerebral palsy based on magnetic resonance imaging," *J. Biomech.*, vol. 40, no. 3, pp. 595–602, 2007.

[36] H. W. Lilliefors, "On the Kolmogorov–Smirnov test for normality with mean and variance unknown," *J. Amer. Statist. Assoc.*, vol. 62, no. 318, pp. 399–402, 1967.

[37] T. I. Carter *et al.*, "Accuracy and reliability of three different techniques for manual goniometry for wrist motion: A cadaveric study," *J. Hand Surgery*, vol. 34, no. 8, pp. 1422–1428, 2009.

[38] A. Thibaut, C. Chatelle, E. Ziegler, M.-A. Bruno, S. Laureys, and O. Gosseries, "Spasticity after stroke: Physiology, assessment and treatment," *Brain Injury*, vol. 27, no. 10, pp. 1093–1105, 2013.